Cement and Concrete Research 38 (2008) 1325–1335

Contents lists available at ScienceDirect

Cement and Concrete Research

journal homepage: http://ees.elsevier.com/CEMCON/default.asp

Investigation on key properties controlling early-age stress development of blended cement concrete

Ivindra Pane [a,*], Will Hansen [b]

[a] Department of Civil Engineering, Bandung Institute of Technology, Ganeca 10, Bandung 40132, Indonesia
[b] Department of Civil and Environmental Engineering, University of Michigan, Ann Arbor MI 48109, USA

ARTICLE INFO

Article history:
Received 9 May 2006
Accepted 5 May 2008

Keywords:
Aging
Hydration
Creep
Relaxation
Early-age
Autogeneous
Shrinkage
Strength

ABSTRACT

Age dependent mechanical and kinetic properties including Young's modulus, early-age creep, autogeneous and thermal deformations, and heat of hydration were investigated for concrete made of blended cements. These are among the key properties that control the early-age cracking behavior in hydrating concrete members. Among the main goals of the investigation were to provide the experimental data and to study the effect of adding mineral additives such as fly ash (FA), ground granulated blast furnace slag (GGBF), and silica fume (SF) on the aforementioned properties. The age-dependent behavior of Young's modulus, creep compliance, and autogeneous shrinkage as functions of heat of hydration were modeled. We emphasized on mathematical modeling the viscoelastic properties of concrete. The equations obtained can be used as inputs needed to calculate the early-age stress development in concrete members.

1. Introduction

Temperature change and self-desiccation take place in concrete during early ages where hydration occurs more rapidly. These behaviors are followed by some dimensional changes including thermal dilation/contraction and autogeneous shrinkage. The former comes from the temperature variation inside concrete due to heat generated during hydration and the ambient temperature variation. The latter is produced from the volumetric changes of reacting phases before and after hydration. Such changes are followed by a decrease in capillary pore pressure and a decrease in solid surface energy. Both processes act as the driving force for shrinkage. If the thermal and autogeneous deformations are high enough and restrained due to the boundary conditions, stresses can develop internally. When such stresses exceed concrete strength, which is still relatively low at early ages, cracking may occur. This problem has received some attention recently, and is often called the early-age cracking. As our understanding about it is still developing, it is necessary to investigate the key properties that control this behavior.

The early-age cracking is often observed in structures made with low water cement to water ratio concrete which is a characteristic of high-strength concrete. Within the last few decades, it has been recognized that autogeneous deformation/shrinkage is larger in concrete with low water to cement ratio and in concrete made with silica fume [1–3]. However, due to their economical benefits mineral additives such as fly ash, silica fume, and ground blast furnace slag have been used in blended cements to improve the resistance against long term environmental conditions such as chloride attacks [4] and freeze–thaw cycles [5]. Generally speaking, long term concrete performance is strongly affected by its short term counterpart as concrete will have to survive the early-age problems in order to guaranty a good long term behavior. This makes it necessary to look at the short term behavior like the early-age cracking, especially in blended cement concrete.

Early-age stresses develop with time and involve time dependent properties like creep and other mechanical properties that are strongly influenced by hydration such as strength and Young's modulus [6–10]. Several studies have been dedicated to investigating creep behavior of concrete which have included looking at the difference between compressive and tensile behaviors [11–16]. Some of these studies have been conducted to obtain early-age creep properties [6,15,16]. From [13,14], concrete creep under tension and compression were also known to be different. Creep in tension was about 20% higher than creep in compression. Analyzing the risk of cracking at early ages favors the use of tensile creep since concrete cracks under tension at early ages.

Sources of early-age deformations are temperature change and self-desiccation. The deformations caused by both factors above are influenced by hydration. Self-desiccation behavior has been found to

* Corresponding author. Tel.: +62 22 251 0715.
E-mail address: ivpane@netscape.net (I. Pane).

0008-8846/$ – see front matter © 2008 Elsevier Ltd. All rights reserved.
doi:10.1016/j.cemconres.2008.05.002

relate closely to degree of hydration and the type of cement [17,18]. Temperature change in concrete during early ages occurs naturally from the heat produced by hydration and its transfer to the surrounding. As the deformation and the time dependent properties (creep) relevant to the early-age stress development are closely related to hydration it is important to study how hydration evolves with time and the factors influencing it. Among these factors, temperature is noted to be the most important one as it significantly alters the hydration rate during the first few days [15,19–22]. In addition, its influence is also observed in some key concrete properties such as compressive strength and Young's modulus [21,23,24].

This investigation focuses on obtaining key material properties that control the development of early-age stresses in concrete members. These include: heat of hydration, compressive and tensile strengths, Young's modulus, creep compliance, relaxation modulus, coefficient of thermal expansion, and autogeneous deformation. The main objective is to provide experimental inputs necessary for predicting the early-age stress development. In doing so, it is necessary to correlate the aging characteristics of the aforementioned concrete properties with a measure of hydration and to develop mathematical models of properties versus hydration. The emphasis is on modeling the viscoelastic properties (creep compliance and relaxation modulus) of the concrete mixes studied. The obtained correlations and models are then used as inputs for predicting the early-age stress development which is discussed in detail in the accompanying paper [25]. To provide a thorough study, effects of temperature on properties development are incorporated through their dependencies upon hydration. A hydration model that is capable of taking into account the influence of temperature has been developed for this purpose.

2. Experiments

2.1. Materials and mixes

In this work, a total of eight concrete mixes were tested. Two water to binder ratios (w/b) considered, 0.35 and 0.45, were thought quite common in practice. For instance, concrete with w/b=0.35 is often used for bridge decks and w/b=0.45 is widely used for concrete pavement slabs. Binder and mineral additives used were: ordinary Portland cement type I (OPC), fly ash class F (FA), ground granulated blast furnace slag (GGB), and silica fume (SF). Natural glacial gravel (gradation 6AA according to Michigan Department of Transportation classification) and class II sand (Michigan Department of Transportation classification) were used as coarse and fine aggregates. The mixes, as shown in Table 1, contain 25% FA, 25% GGBF, and 10% SF (cement replacement by weight). Each mix is labeled according to its w/b. These proportions can be considered moderate and common in practice for users of FA, GGBF, and SF. Compositions of Portland cement type I together with the additives are provided in Table 2. In all concrete mixes the binder content was kept fixed at 350 kg/m^3.

Tests were performed to obtain: isothermal heat of hydration (Q), compressive strength (f_c'), split tensile strength (f_{sp}), Young's modulus (E), tension creep compliance (J), autogeneous deformation (ε_{au}), and coefficient of thermal dilation (CTD). These tests, except the measurement of heat of hydration, were performed for concrete and are summarized in Table 3. The heat of hydration was measured for paste samples. In relating the heat of hydration of concrete to that of cement paste it is assumed that the heat of hydration of cement paste in concrete is the same as that of the paste alone. By that, it is implicit that the coarse and fine aggregates in concrete are considered inert against hydration reaction. Determinations of f_c', f_{sp}, E, J, and CTD were done at several ages while ε_{au} and Q were measured continuously.

Table 1
Mix design information

Mix no.	% OPC I	% Additive	w/b
45-1	100	0	0.45
45-2	75	25 (FA)	0.45
45-3	75	25 (GGB)	0.45
45-4	90	10 (SF)	0.45
35-1	100	0	0.35
35-2	75	25 (FA)	0.35
35-3	75	25 (GGB)	0.35
35-4	90	10 (SF)	0.35

Table 2
Binder compositions

Compound (%)	OPC I	Fly ash	GGBF	SF
SiO_2	20.4	57.4	37.5	94.5
Al_2O_3	5	18.2	7.8	0.3
Fe_2O_3	2.5	5.3	0.4	0.9
CaO	62.4	8.3	38	0.5
MgO	3.4	3.7	10.7	0.9
SO_3	2.8	0.9	3.2	–
Na_2O	0.3	1.14	0.3	–
K_2O	0.7	1	0.5	–
TiO_2	–	1.2	0.4	–
P_2O_5	–	0.36	–	–
Mn_2O_3	–	–	0.6	–
SrO	–	0.7	0.1	–
ZnO	–	0.1	–	–
Loss on ignition	2.6	0.2	0.6	1.9

% Weight	C3S	C2S	C3A	C4AF	Blaine (cm^2/g)
OPC I	53.7	18	9.1	7.6	4290

2.2. Split tensile strength and Young's modulus

The split tensile strength, and Young's modulus were determined using a servo-hydraulic compression testing machine at seven different ages: 0.5–0.8, 1, 2, 3, 7, 28, and 90–120 days. Two concrete specimens were measured at each age. The same specimens were used to determine both the Young's modulus and compressive strength, the former one first followed by the latter. The specimens tested were all cylindrical, measuring 100 mm (4 in.) in diameter and 200 mm (8 in.) in length. The elastic displacements in the determination of Young's modulus were measured using two 50 mm gauge extensometers attached on two opposite sides of the specimen. All specimens were cured in lime-saturated water at 22.5 to 23 °C starting from 12 h after casting and remained in the curing tank until they were ready for testing.

2.3. Heat of hydration

The detail of heat of hydration measurement has been given in a separate paper by the authors [26]. Briefly, the test was done in isothermal condition at three curing temperatures: 15, 23 and 34 °C. The purpose of doing so was to generate necessary inputs for

Table 3
Summary of test information

Test/properties	Curing condition	Age of testing (h)
f_c', f_{sp}, and E	Wet (lime-saturated solution)	12–18, 24, 48, 72, 168, 672, >2160
Creep	Sealed	24–26, 72, 168, 336
Autogeneous deformation	Sealed	After casting to 7 days
Heat of hydration	Sealed	After casting to 21 days

calculating the heat of hydration under any prescribed temperature histories. The measurement was performed for three weeks in which the rate of heat could still be accurately recorded. Beyond that period the rate became very low and difficult to measure accurately.

2.4. Coefficient of thermal expansion

The coefficient of thermal dilation of concrete was determined using a specially designed system consisting of a frame made of invar steel, a circulating water bath, and a heating–cooling controller. The schematic drawing of the frame is given in Fig. 1. The specimen can be rectangular or circular in cross section. The maximum height allowed for the specimen was 300 mm (12 in.) and the maximum diameter or cross sectional length allowed was 150 mm (6 in.).

Two specimens can be tested simultaneously in the water bath. The value of CTD was obtained for wet concrete since the specimens were wet cured prior to measurement. The specimens were tested at ages of 1, 3, and 7 days. During the test, the water temperature was raised from 20 to 35 °C. The displacement of each specimen was measured by an LVDT which was placed according to Fig. 1. Before testing, a stainless steel bar was used to calibrate the frame, and hence, the measurement could be corrected from errors induced by the expansion or contraction of the frame. Each specimen had at least two thermocouples embedded within. One thermocouple must be placed as close as possible to the center of each specimen. At least two thermocouples must be used to measure the water temperature. To examine the system performance, two mature (28 days old) concrete specimens from the present research were tested. Each specimen was tested with the reference steel bar simultaneously. The temperature varied from about 22 to 34 °C. The plots of the strain with temperature obtained for the two specimens showed very linear relation. From the plots, average values of CTE were found to be 12.6×10^{-6}/ °C for concrete and 17.4×10^{-6}/ °C for stainless steel. The value for concrete is within the range reported in literature [27]. Furthermore, CTE for steel is very close to what is found in metal literature, proving the accuracy of the test system.

2.5. Creep

The tensile creep test was performed on two specimens to obtain basic creep compliance (creep without drying effect). The specimen was rectangular in cross section with dimensions of $100\times100\times400$ mm^3 ($4\times4\times16$ in.^{3}). Simultaneously, deformations of two identical load-free specimens were also measured in order to provide corrections due to temperature changes. The load-free specimens were measured on the same frame used to measure CTE. Drying was minimized by sealing the loaded and load-free specimens using 3 to 4 layers of thin plastic foil. Loading was applied mainly at four ages: 1, 3, 7, and 14 days. The load durations were the time lags between each age of load application. Two linear variable displacement transducers (LVDTs) attached on both sides of the specimen were used for each loaded specimen (100 mm gauge length) and one was used for each of the unloaded specimen (300 mm gauge length). The LVDTs used were high precision ones with accuracy (for 100 mm gauge length) of 1 μm strain. The tensile creep test was only performed on concrete. All specimens were cured and tested at 23 °C.

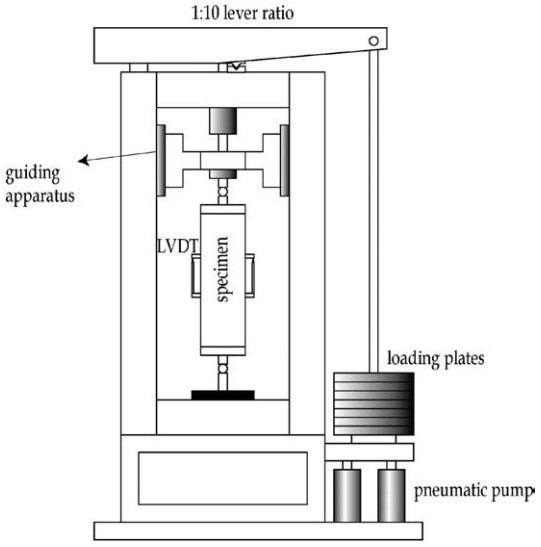

Fig. 2. Tensile creep frame.

The tensile creep frame was a lever type of 1:10 ratio. Each end of the specimen was attached to the loading frame by threaded bars bolted to the steel plates that grip the specimen. Four threaded rods which were connected to a steel plate were embedded at each end of the specimen during casting. To assure proper alignment, a specially designed mold was used for casting. Dead weights were used for loading the specimens. The frame was equipped with a pneumatic loading unit that enabled one to control the rate of loading. In addition, a self-guiding apparatus was mounted to the frame to minimize the eccentricity. These features are shown schematically in Fig. 2. To assure the linear viscoelastic behavior, the maximum load applied was kept below 0.3 f_{sp}.

2.6. Autogeneous deformation

The autogeneous deformation is a stress free deformation due to the change in capillary pore pressure and the change in solid surface energy in sealed concrete. It was measured on concrete specimens using special molds with a temperature control system similar to that used for measuring CTE. The mold, as illustrated in Fig. 3, was equipped with closed channels on both vertical sides. The channels

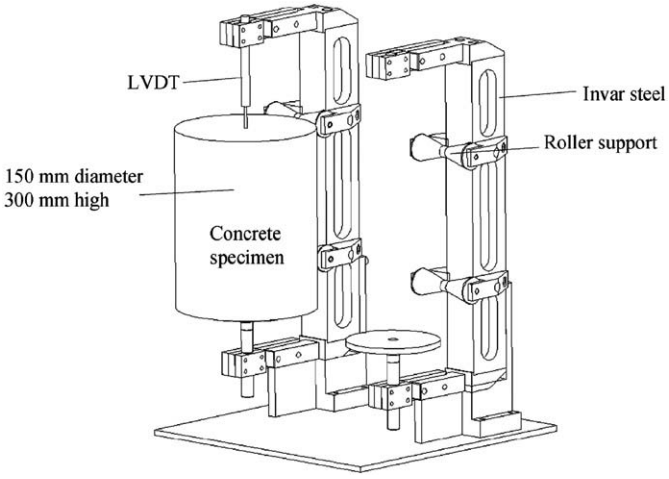

Fig. 1. Testing frame for the coefficient of thermal expansion.

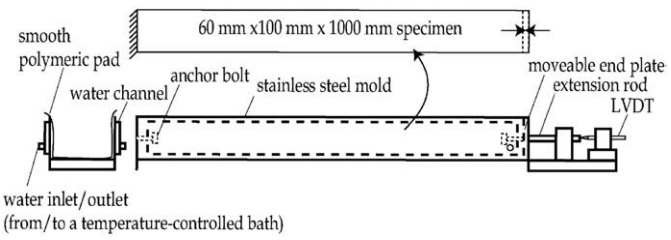

Fig. 3. Autogeneous shrinkage mold.

were used to flow water that maintains the test condition isothermal. Water temperature is maintained constant by a water bath equipped with a heating–cooling controller. The top surface of the specimen is covered with an impermeable plastic sheet to prevent moisture transport.

The autogeneous deformation was measured simultaneously on two specimens and the data reported was the average value obtained from both specimens. The measurement began immediately after casting. Each specimen was 1000 mm long, 100 mm wide, and 60 mm thick. The shrinkage mold was covered by a very compliant rubber pad to minimize frictional restraint. During measurement, each specimen's surface was covered by thin polyethylene sheets to minimize drying. This effort had been proven to be effective as several measurements showed that only about 0.5% out of the total water was lost. The test was terminated after 1 week for most specimens.

3. Hydration kinetics

Degree of hydration of cement is a basic property that can be used to characterize the development of concrete microstructure and thus, its mechanical properties. Heat of hydration represents the bulk thermal energy generated by chemical reactions of cement and pozzolanic materials in blended cements. As it is related to the hydration products formed during hydration, it is directly tied to concrete microstructure and thus, to the mechanical properties of concrete. In this study, the heat of hydration of blended cement has been measured and used to follow hydration. Throughout this paper, heat of hydration of cement in concrete is assumed to be equal to the heat of hydration of cement paste. This means the presence of aggregates does not hinder hydration of cement.

To model the heat development over time, we refer to the previous studies by the authors [28]. Therein, it has been suggested that a three parameter model (TPM) proposed in [29] can accurately model the heat development. The model will be briefly summarized below. TPM is defined as:

$$Q = Q_{0,\infty} \ \exp\left[-\left(\frac{\tau}{t}\right)^{a}\right] \tag{1}$$

In the above equations, t is time, Q and $Q_{0,\infty}$ are heat of hydration and the ultimate heat of hydration, respectively, while τ and a are model parameters. The effect of temperature on degree of hydration and heat of hydration can be incorporated in the three parameters:

$$Q_{0,\infty} = A_0 + A_1 T \tag{2}$$

$$\tau = B_0 e^{-B_1 T} \tag{3}$$

$$a = C_0(1 - C_1 T) \tag{4}$$

Under non-isothermal condition, T becomes $T(t)$. To calculate non-isothermal heat of hydration, T is assumed to be constant within each time increment. Heat is then calculated by integrating the rate of heat and updating T each time. The integration can be performed numerically using, for example, the trapezoidal rule,

$$\frac{dQ}{dt}\Big|_T = \frac{a}{\tau} Q_{0,\infty} \left(\frac{\tau}{t}\right)^{a+1} \ \exp\left[-\left(\frac{\tau}{t}\right)^{a}\right]\Big|_T \tag{5}$$

$$Q(t) = \int_0^t \frac{dQ}{dt}\,dt \approx \sum_{i=0}^{k} \frac{1}{2}\left[\frac{dQ}{dt}\left(t_{i-1/2}, T_{i-1/2}\right) + \frac{dQ}{dt}\left(t_{i+1/2}, T_{i+1/2}\right)\right]\Delta t_i \tag{6}$$

In the above equation, subscribed T means that the quantity is evaluated at a constant temperature. This method has been used in [28] to predict the heat development under semi adiabatic conditions and appeared to be accurate.

Results of the isothermal heat of hydration test are plotted in Fig. 4 for hydration at 23 °C. It is seen from this figure that different blends do not produce the same heat. This indicates the presence of pozzolanic reactions, clinker hydration, and possibly catalytic effects of pozzolans. For instance, silica fume (SF) and blast furnace slag (GGBF) are seen to increase the heat of hydration. The other finding is that the systems with lower w/b produce lower heat of hydration. It is consistent with the fact that the space where hydration products can grow is limited in lower w/b systems. Heat of hydration curves at other temperatures is not shown as it was found to exhibit similar trends. The modeling parameters (A_i, B_i, and C_i) in Eqs. (2), (3), and (4) necessary to apply the method above can be obtained from the heat data. They are summarized in the paper by the authors [25] accompanying this study.

4. Early-age viscoelastic properties

4.1. Young's modulus

Young's modulus data can also be fitted by TPM. The strong age dependency of this property has been well known [6–10]. Its relations to hydration have been explored, especially for the computation of stresses at early ages.

The correlation between normalized heat of hydration and Young's modulus is shown in Fig. 5 for w/b=0.35. The heat data have been normalized by the predicted ultimate values, $Q_{0,\infty}$, in order to compare the property development of one mix relative to others at the same level of hydration. This is necessary since different types of binder do not necessarily produce the same hydrates or the same amount of heat per unit weight of binder. As a consequence, the comparison of one property at the same amount of heat is not the same as comparing it at

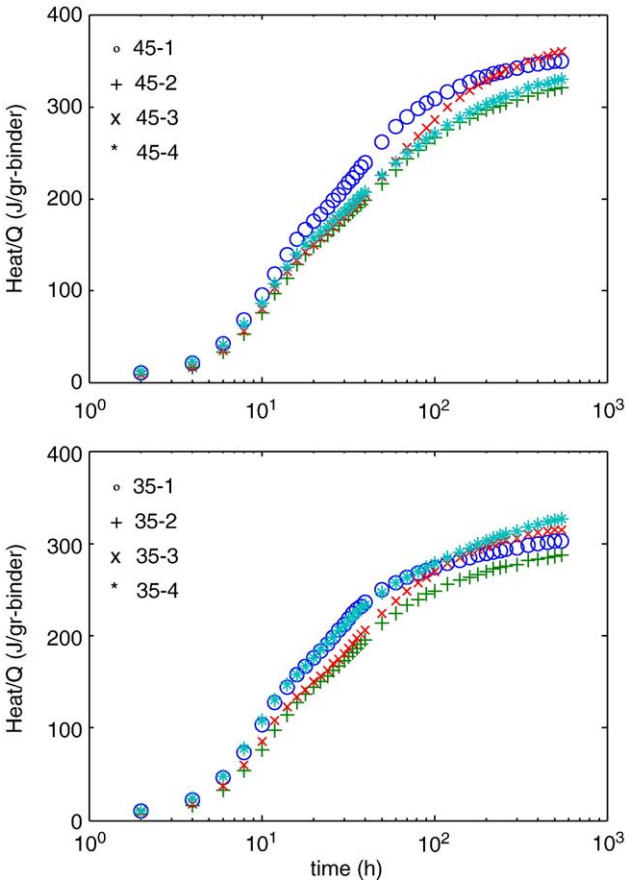

Fig. 4. Isothermal heat of hydration at T=23 °C.

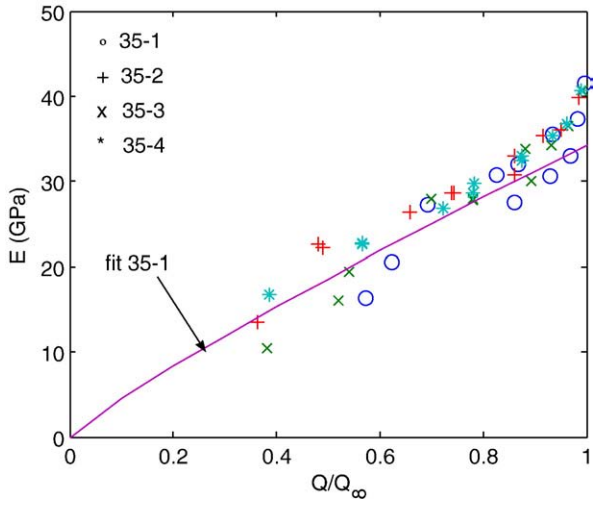

Fig. 5. Young's modulus development.

the same level of hydration. Since heat of hydration was measured only up to 21 days while strength and Young's modulus were measured up to 90–120 days, it is necessary to extrapolate the heat data to 90–120 days. This is done using Eq. (7) below.

The result shown in Fig. 5 indicates that for the systems investigated, only the silica fume concrete shows slightly higher strengths. The other systems seem to gain strengths similarly. This was also observed in the other mixes with w/b=0.45. The shapes of Young's modulus seem to suggest a power relation between E and Q/Q_∞. Therefore, the following equation can be used to express $E(Q)$,

$$E = k_1 \left(Q/Q_{0,\infty}\right)^{k_2} \tag{7}$$

where k_1 and k_2 are constants.

4.2. Models for creep compliance and relaxation modulus

To better understand the viscoelastic behavior of the concrete mixes, it is necessary to write the creep compliance of concrete the following form [30]:

$$J(t,t') = \frac{1}{E(t')}\left[1+\phi(t,t')\right] \tag{8}$$

where $\phi(t,t')=E(t')C(t,t')$ is called the specific creep and $C(t,t')$ is called the creep coefficient. The specific creep is essentially the time dependent strain per unit stress in excess of the instantaneous elastic strain. The creep coefficient is the time dependent strain per unit instantaneous or elastic strain in excess of the elastic strain itself. Typical creep data plotted as creep coefficient for various mixes are shown in Fig. 6. We first model these creep data and perform numerical inversion to obtain relaxation modulus, which will be modeled as well. Then, characteristics of the creep compliance and the relaxation modulus are discussed by referring to their model parameters.

There are many empirical models for creep compliance of concrete. We seek for a simple yet accurate model with the least number of parameters. The particular aging creep compliance chosen in this study is the log-power creep law [11] which is written as:

$$J(t,t') = \frac{1}{E(t')} + C(t,t') = \frac{1}{E(t')} + q_1 \ \ln\left[1+q_2(t')(t-t')^n\right] \tag{9}$$

The log-power creep law has been shown to be simple and accurate as opposed to for instance, the double-power law that may produce unrealistic/negative relaxation [11]. It also requires minimum model parameters q_1, q_2, and n. Results of curve-fitting and the accuracy of the above equation can be seen as solid lines in Fig. 6. Analyzed data indicates that for each mix, q_1, and n can be fixed as constants while the parameter q_2 must be varied with the age. By

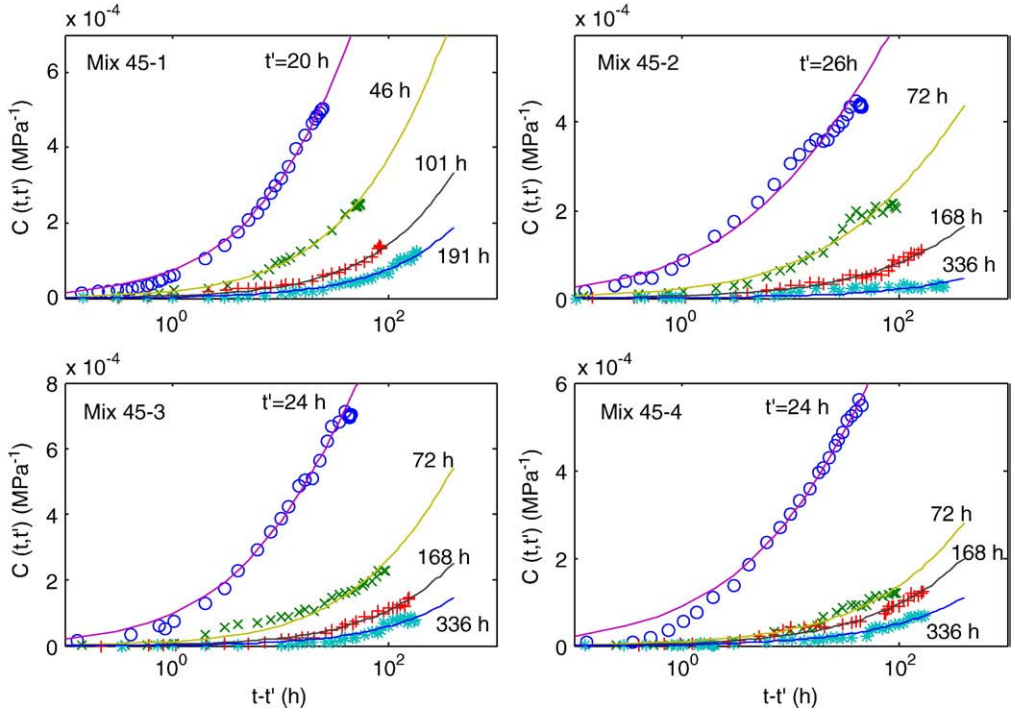

Fig. 6. Creep data and curve fits, w/b=0.45.

doing this, it can be seen from Fig. 6 that Eq. (9) provides highly accurate predictions.

In order to obtain the relaxation modulus, the age-dependent parameter q_2 must be interpolated by a smooth function. In this work, the following power equation was chosen:

$$q_2(t') = c_1 t'^{-c_2} \tag{10}$$

where t' is the age of concrete, and c_1 and c_2 are constants. A more detailed discussion about the variation of q_2 with age and hydration will be provided later. The relaxation modulus $R(t,t')$ was obtained after solving numerically the Volterra integral equation:

$$1 = \int_0^t J(t,t')dR(t') \tag{11}$$

using the trapezoidal integration scheme. Unlike the creep compliance, models for the relaxation modulus of concrete are rarely proposed. Morimoto and Koyanagi [31] for instance proposed a logarithmic-type relaxation modulus while Emborg [6] and Bazant [11] used the Dirichlet series. The latter is also used in this study and will be presented subsequently. Here, we propose a hyperbolic function:

$$R(t,t') = m_1(t')\left[1 - \frac{[(t-t')/m_2(t')]^p}{1+[(t-t')/m_2(t')]^p}\right] \tag{12}$$

to fit the numerically obtained $R(t,t')$. The numerical results together with the results of curve-fitting using Eq. (12) are shown in Fig. 7, where solid lines indicate the fits. In the above equation, it suffices to set m_2 as the aging parameter, while m_1 is essentially the Young's modulus which has been modeled earlier. The variation of m_2 with time can also be accurately fitted by a power equation:

$$m_2(t') = d_1 t'^{d_2} \tag{13}$$

Its variation with age and hydration will be discussed later. With the aforementioned parameters, the resulting predictions by Eq. (12) appear to be very precise. The other option is to fit the relaxation modulus with an exponential-type function similar to the one used for the heat of hydration. However, for it to be as accurate as the hyperbolic function above, more age-dependent parameters are needed. Another reason for avoiding such an exponential-type function will be explained subsequently, when the thermodynamic argument is used to check the validity of the chosen relaxation function.

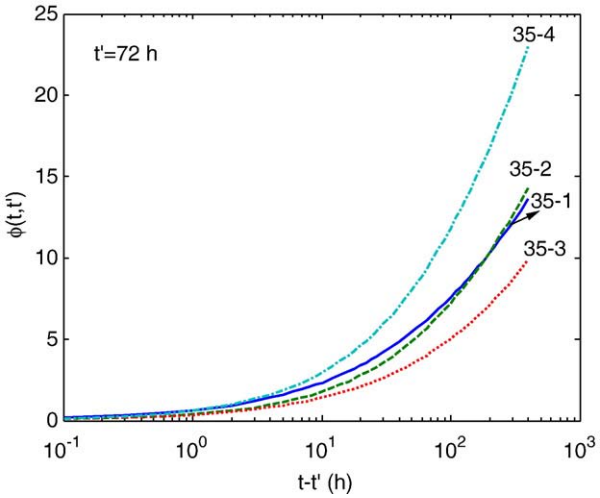

Fig. 8. Modeled specific creep at age=72 h.

It is instructive to see the effect of additive on creep and relaxation behavior. However, the analysis made here is limited to the concrete response by a step loading at a certain age. More thorough analysis on the response by a loading history is presented in the other work by the authors [25]. As it describes the magnitude of the creep strain relative to the elastic strain, effects of mineral additive on creep will be examined in terms of specific creep $\phi(t,t')$. Fig. 8 illustrates how $\phi(t,t')$ at the age of 72 h varies with the loading time. Since all concrete were

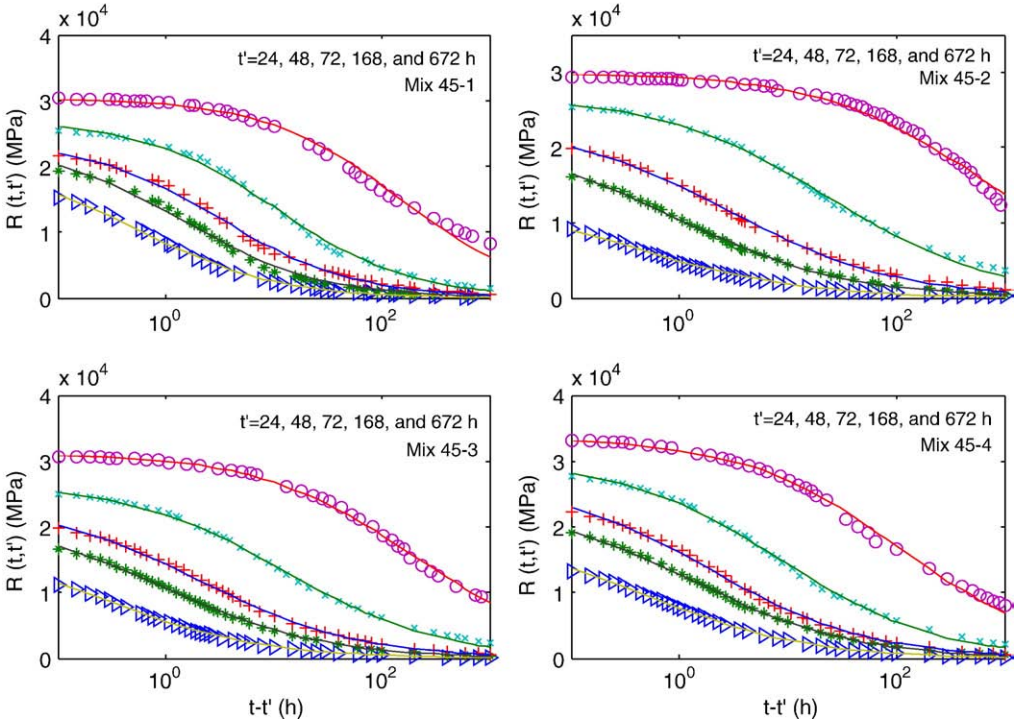

Fig. 7. Calculated relaxation and curve fits, w/b=0.45.

made of the same aggregates and had the same binder content, any variations of creep from one mix to the others would be caused by the binder. For the age of 72 h (3 days), the presence of SF seems to induce more early creep, while the presence of GGB tends to lower the magnitude of creep. Effects of additive on the relaxation modulus can be seen in Fig. 9. As in the case of creep, the relaxation modulus must be first normalized by the Young's modulus. Such a normalization allows us to see how the stress in each mix relaxes from the same initial value. It is seen that concrete containing SF relaxes more rapidly than any other mixes. Relaxation of concrete containing FA and GGB do not seem to significantly differ from OPC concrete. The observed influence of SF to creep is rather difficult to explain. The present study focuses on reporting the observed effect. However, if one is to speculate the effect of SF is to alter creep micromechanisms such as the movement of the interlayer water present in the hydration product and the hydration process itself, which are thought to be the source of the aging viscous behavior of concrete [11].

4.3. Representations by Dirichlet series

The creep compliance and relaxation modulus can also be modeled by the Dirichlet or Prony series. The Dirichlet series is often used for the calculation of stress/strain in general viscoelastic bodies. It allows for solving the viscoelastic problem in the form of differential equations [11,12]. When the creep compliance is expressed by Eq. (9), the stress/strain history must be integrated incrementally and the aging coefficients must be updated in each increment. Such a method requires the storage of all stress history from the beginning of the application of load. Here, the Dirichlet series representations are provided as an alternative to the log-power creep law and the hyperbolic-type relaxation modulus. They can be used as inputs when the viscoelastic stress or strain is to be solved in the form of differential equations. Since they are quite important, the Dirichlet series representations are analyzed in detail here.

Representations of the creep compliance and the relaxation modulus are written as [11]:

$$J(t,t') = \sum_{\mu=1}^{k} \frac{1}{D_\mu(t')}\left[1-e^{(t-t')/\tau_\mu}\right] \tag{14}$$

$$R(t,t') = \sum_{\mu=1}^{k} E_\mu(t')e^{(t-t')/\tau_\mu} \tag{15}$$

where D_μ and E_μ are respectively, the aging parameters similar to the compliance and the modulus, and τ_μ is the retardation time. As

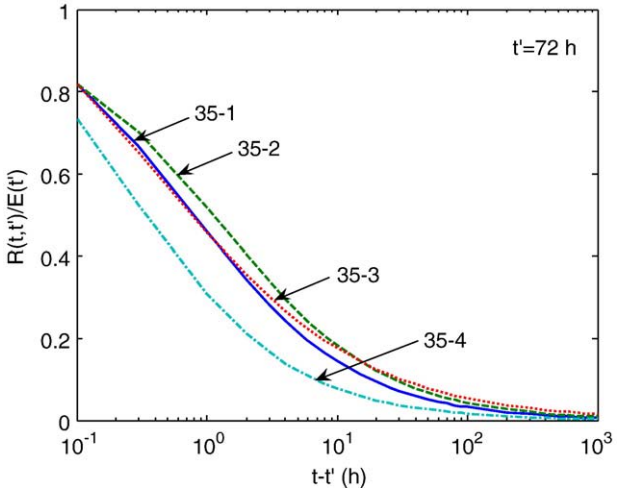

Fig. 9. Modeled normalized relaxation at age = 72 h.

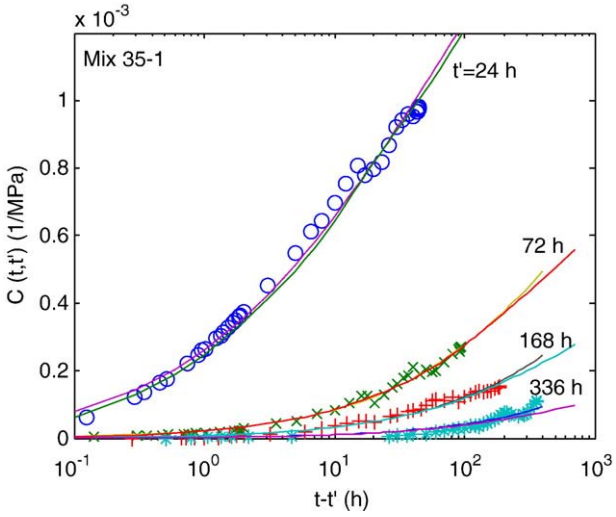

Fig. 10. Dirichlet series representation of creep function (dashed lines is the log-power approximation).

suggested in [12], τ_μ can be equally spaced in the logarithmic axis and thus, can be determined using the following form:

$$\tau_\mu = 10^{\mu-1}\,\tau_1 \tag{16}$$

where τ_1 can be found from the point where the creep curve plotted in $\log(t-t')$ scale begins to rise. The instantaneous or elastic modulus is calculated by fitting Eq. (14) to the age-dependent Young's modulus after setting $\tau_{\mu=0}$ several magnitudes smaller than $\tau_{\mu=1}$, e.g. $\tau_0 = 10^3\,\tau_1$.

The aging parameters D_μ and E_μ are usually obtained using the least square minimization. However, such a method often leads to negative values and as a consequence, the thermodynamic restriction on creep compliance is violated [32]. In this study, another method based on the asymptotic series expansion of Laplace transformation was employed. This approximation has been discussed and used in [33,34]. The objective is to calculate the continuous form of D_μ and E_μ in terms of the continuous retardation spectrum $L_\square$. The derivation of this method can be found in [33]. For a given creep compliance or creep coefficient $C(t,t')$, the continuous retardation spectrum is:

$$L(\tau) = -\lim_{k\to\infty} \frac{(-k\tau)^k}{k-1} C^{(k)}(k\tau) \tag{17}$$

where τ is now the continuous retardation time, $C^{(k)}$ is the kth derivative of function C, and k must be larger than one. The discrete values of $D_\square$ and $E_\square$ are calculated from

$$\frac{1}{D_\mu} = L(\tau)\ \ln\ 10 \times \Delta(\ \log\ \tau_\mu) \tag{18}$$

$$\mathrm{E}_\mu = -L(\tau)\ ln\ 10 \times \Delta(\ log\ \tau_\mu) \tag{19}$$

The interval $\Delta(\log \tau_\mu)$ can be safely set to log 10 = 1 [33]. The above method can be used to determine the age-dependent moduli by calculating the moduli at different ages and interpolating the values using some smooth functions.

As in the case of q_2 in the log-power creep, $D_\mu(t')$ can be accurately fitted by a power equation:

$$D_\mu(t') = e_1 t'^{e_2} \tag{20}$$

for each value of retardation time. On the contrary, E_μ cannot be fitted accurately by a simple function. Even if it can be fitted, the function used will be very lengthy and contain too many parameters. Therefore, it is not represented by other than the approximation above.

The Dirichlet series representations of creep data, as indicated by solid lines, are shown in Fig. 10 together with the log-power creep law. In this figure, the series consist of five terms. The result of the asymptotic approximation appears to be accurate, almost as accurate as the log-power creep law but with less than perfect match. The result of the approximation for the relaxation modulus is shown in Fig. 11. As indicated by solid lines, the Dirichlet series representations are not as good as in the case of creep. Seven terms are needed in the series. It appears that due to significant change in relaxation, the number of terms needed to produce quite accurate series increases. In the above calculation, the order of the asymptotic expansion (index k) is set to three, for either the creep or the relaxation function.

In this study, a direct determination of D_μ and E_μ by the least square method does not produce completely non-negative values. On the other hand, the values obtained using the asymptotic approximation are not. However, this may not apply for all relaxation functions. For example, an exponential-type function,

$$R(t,t') = m_1(t')\left[1 - exp\left(-\left[\frac{m_2(t')}{t-t'}\right]^p\right)\right] \tag{21}$$

is able to produce a very good fit of the relaxation data. Yet in this study, it was found to produce negative values of $E_\square$. The thermodynamic argument of non-diverging relaxation modulus requires that [32]

$$\frac{\partial^2 R}{\partial t \partial t'} = -\sum_{\mu=1}^{k}\left[\frac{\dot{E}_\mu}{\tau_\mu^2}(t') + \frac{E_\mu}{\tau_\mu}(t')\right] e^{(t-t')/\tau_\mu} 0 \tag{22}$$

which obviously requires

$$\frac{\dot{E}_\mu}{\tau_\mu^2}(t') + \frac{E_\mu}{\tau_\mu}(t') > 0 \tag{23}$$

Some negative values of E_μ may not always result in the violation of (23), but it is not realistic according to the solidification theory [32]. Fig. 12 showing the plots of Eq. (23) suggests that the result of the asymptotic approximation above is satisfactory. As for the creep compliance the non-divergence argument reads [11]:

$$\frac{\partial^2 J}{\partial t \partial t'} > 0 \tag{24}$$

which will always be satisfied by guarantying the non-negativeness of D_μ. As will be shown later, the plots of D_μ against t' satisfy this requirement (shown in Fig. 15 below).

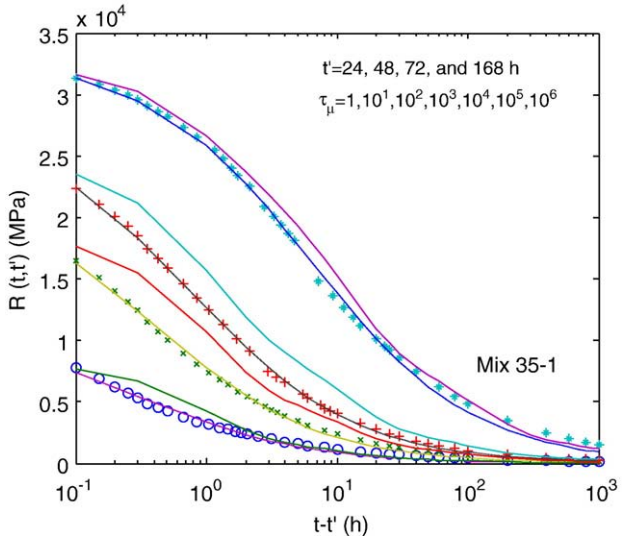

Fig. 11. Dirichlet series representation relaxation function (dashed lines is the hyperbolic approximation).

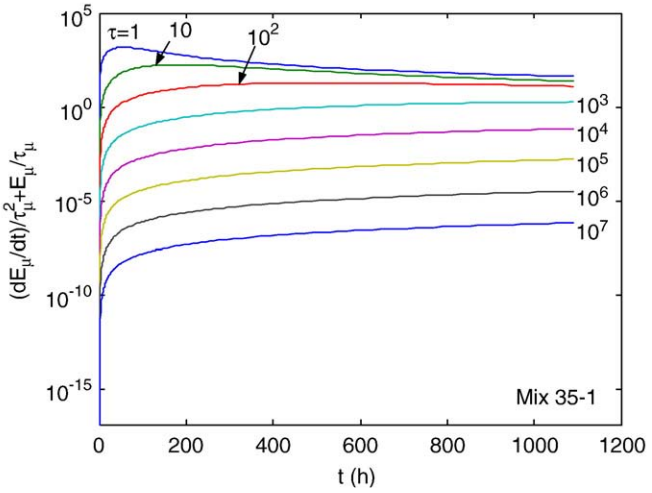

Fig. 12. Variations of $\dot{E}_\mu/{\tau_\mu}^2 + E_\mu/\tau_\mu$ with age.

4.4. Correlations of aging parameters with heat of hydration

Variations of aging parameters q_2, m_2, $D_\square$ and E_μ are shown in Figs. 13–16. Each figure is a pair, the first one shows the variation with age and the second one with heat of hydration. The latter has been

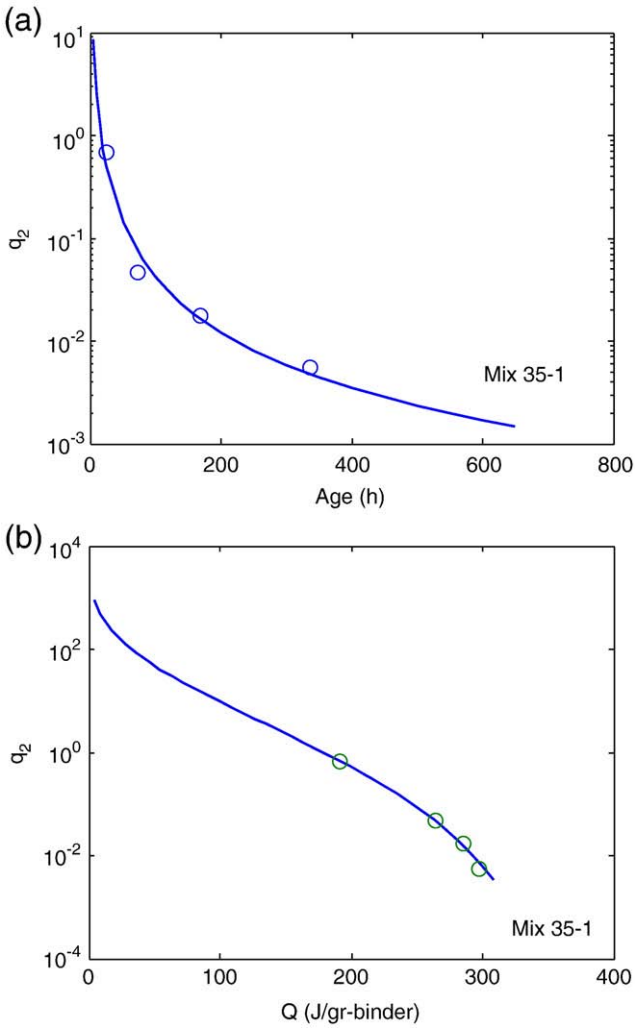

Fig. 13. Variation of parameter q_2 with age and degree of hydration.

chosen since it is the major source of aging and microstructural changes in concrete. It is hard to interpret the physical meaning of q_2, m_2, $D_{\square}$ and E_μ as they tend to be some mathematical functions that describe aging.

Finding the most accurate functions that can fit age-dependent material parameters so that the age (t') can be replaced by heat of hydration (Q), is not trivial. The most logical approach is to invert the time variable in the heat equation (1) and substitute it with (t'). Since all aging parameters in Eqs. (10), (13), and (20) are power type equation, after some generalization, this leads to:

$$\chi(Q) = \alpha\left(\ln\ \frac{\beta}{Q}\right)^{\gamma} \tag{25}$$

where χ can be q_2, m_2, D_μ.

The fit for each parameter obtained using the general form (25) is also shown as solid lines. The relations between creep and relaxation parameters, and heat of hydration are assumed unique, just like the relations between other mechanical properties and heat described above.

5. Autogeneous and thermal deformations

Autogeneous strains of different concrete mixes as functions of time are illustrated in Fig. 17. The magnitudes of strain are, as expected, higher for mixes with lower w/b [17]. The deformation history observed in Fig. 17 indicates that during the early period, some concrete mixes undergo expansion possibly associated with early formation of expansive hydration products (possibly ettringite) [35,36]. From Fig. 17, the expansion is more pronounced in the mixes having w/b=0.45. It is most likely due to the higher capillary pore space available in the mixes with w/b=0.45.

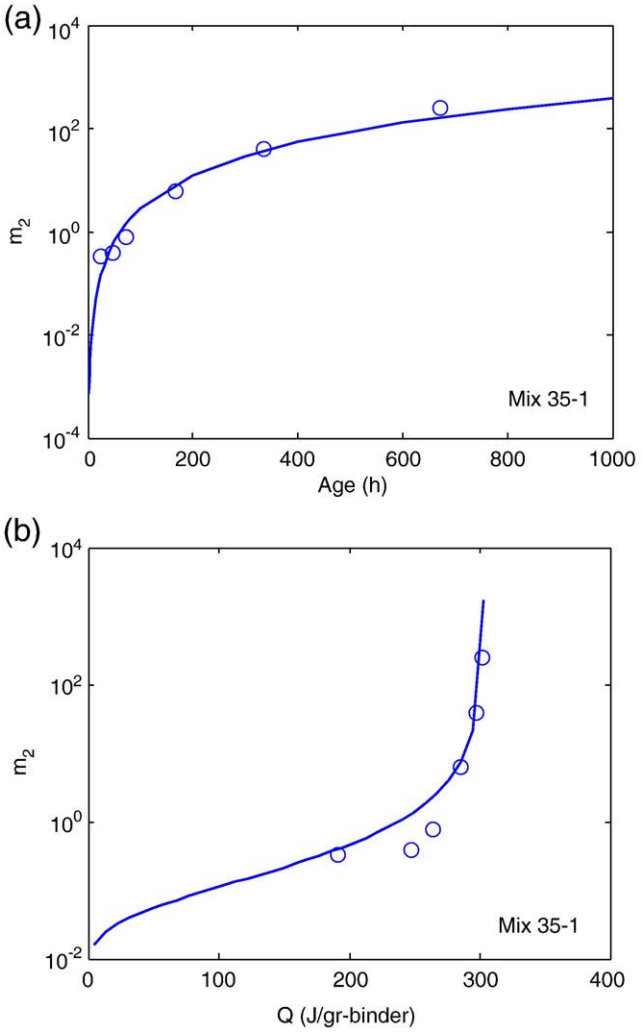

Fig. 14. Variation of parameter m_2 with age and degree of hydration.

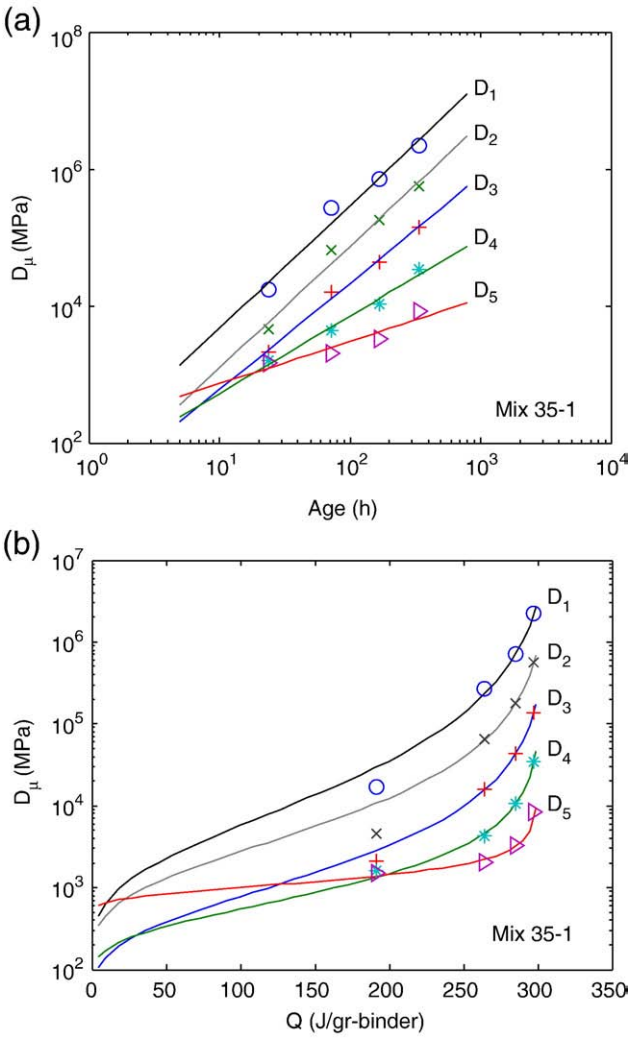

Fig. 15. Variations of D_μ with age and heat of hydration.

The expansive behavior is not necessarily beneficial in the context of early-age stress development. Because the stress generated from restrained autogeneous deformation depends on the viscoelastic properties and hydration. It is very possible that the stress starts to develop after the expansion has ceased and thus, leaving only the contribution of shrinkage deformation.

Relations between autogeneous strains and concrete hydration, as represented by Q, are illustrated in Fig. 18. In showing such relations, the heat of hydration of paste has been assumed to be the same as the heat of hydration of concrete. Such relations appear to be very similar to what found in [17] for the autogeneous shrinkage of paste. For stress calculations that will be presented in the accompanying paper, polynomials of order three or higher can be used to describe autogeneous strains as functions of heat of hydration.

Values of coefficient of thermal dilation (CTD) obtained for different mixes are listed in Table 4. Each value is obtained from two identical specimens. There seems to be no clear trend found for CTD values measured at various ages, although in general CTD tends to be higher in younger specimens. A somewhat similar finding was reported in

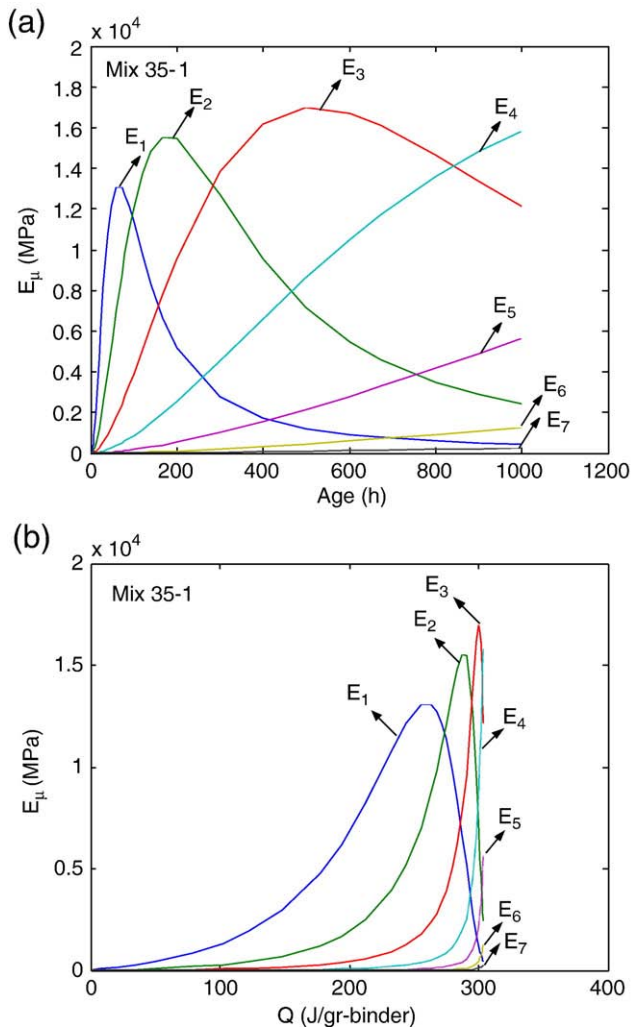

Fig. 16. Variations of E_μ with age and heat of hydration.

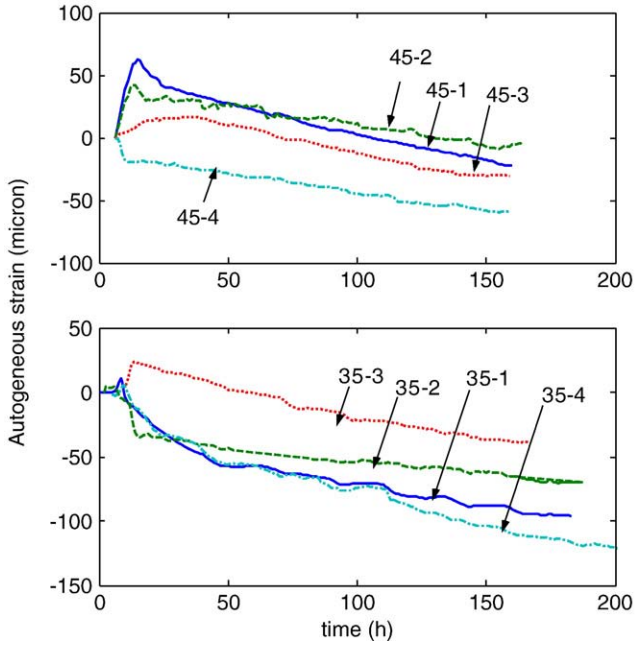

Fig. 17. Autogeneous deformation as a function of time.

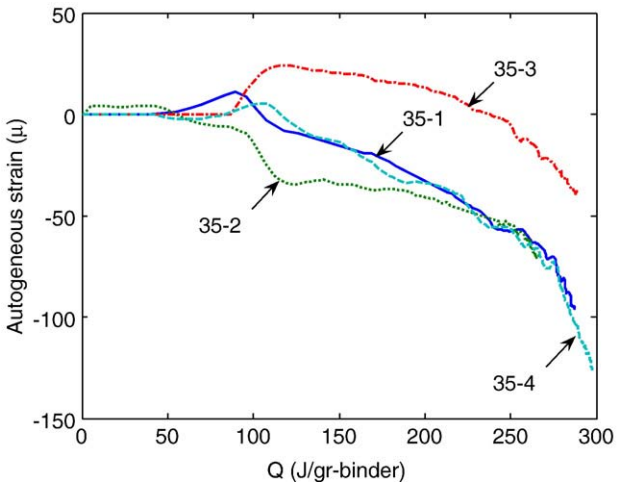

Fig. 18. Autogeneous deformation as a function of heat.

[37,38], where CTD was found to change dramatically between the age of 6 to 20 h but did not vary significantly after 20 h.

From Table 4, the effect of w/c is also found to be minor. Also, the average CTD does not vary significantly from one mix to another. Based on the results presented CTD can be approximated to be age independent and only the average value is used for each mix.

6. Conclusions

Relations between several important concrete properties such as compressive strength, split tensile strength, Young's modulus, creep compliance, relaxation modulus, autogeneous deformation, and coefficient of thermal dilation, with degree of hydration have been presented in this paper. These properties are needed to assess the risk of early-age cracking and for predicting the stress development at early ages. Findings presented in this paper suggest that mechanical properties including Young's modulus, and autogeneous deformation relate uniquely to heat of hydration. For these properties, heat of hydration can be used as an aging parameter. Furthermore, effects of temperature on these properties can be incorporated through the calculation of heat of hydration. Different mineral additives produce different creep and autogeneous deformation properties. In particular, concrete containing silica fume (SF) seems to have greater early-age creep than the ordinary concrete, but at the same time also exhibits more autogeneous shrinkage.

The measured properties, especially the aging and viscoelastic ones, have been modeled mathematically. The proposed viscoelastic models have been shown to satisfy the thermodynamic requirement. The models result in parameters that can be used to accurately describe and capture the behavior of different concrete mixes. The most important feature of the models is that the aging parameters have been related to the heat of hydration. The latter can be used as a general measure of concrete hydration under different thermal history.

The next step is to investigate the development of stress in hydrating concrete, especially at early ages. The data and models

Table 4
Values of coefficient of thermal dilation (CTD) (10^{-6}/ C)

Age (h)	45-1	45-2	45-3	45-4	35-1	35-2	35-3	35-5
24	10.07	8.41	12.51	10.86	11.11	12.09	10.06	9.21
72	12.60	11.14	9.14	7.92	9.49	9.16	9.17	9.87
168	9.11	7.72	9.56	8.56	8.63	9.13	8.85	8.23
Average	10.59	9.09	10.40	9.11	9.74	10.12	9.36	9.10

provided serve as very valuable inputs that can predict the stress development. It is expected that variations of the experimentally-derived model parameters can provide important information on how different concretes behave at early ages.

References

[1] Z. Jiang, Z. Sun, P. Wang, Autogeneous relative humidity change and autogeneous shrinkage of high-performance cement pastes, Cem. Concr. Res. 35 (8) (2005) 1539–1545.
[2] Y. Yang, R. Sato, K. Kawai, Autogeneous shrinkage of high-strength concrete containing silica fume under drying at early ages, Cem. Concr. Res. 35 (3) (2005) 449–456.
[3] A. Loukili, A. Khelidj, P. Richard, Hydration kinetics, change of relative humidity, and autogeneous shrinkage of ultra-high-strength concrete, Cem. Concr. Res. 29 (4) (1999) 577–584.
[4] R.K. Dhir, M.A.K. El-Mohr, T.D. Dyer, Developing chloride resisting concrete using PFA, Cem. Concr. Res. 27 (11) (1997) 1633–1639.
[5] G.G. Litvan, P.J. Sereda, Particulate admixture for enhanced freeze–thaw resistance of concrete, Cem. Concr. Res. 8 (1) (1978) 53–60.
[6] M. Emborg, Thermal stresses in concrete structures at early ages, Doctoral Thesis, Lulea Univ. of Tech. (1989).
[7] A. Gutsch, F.S. Rostasy, Young Concrete under High Tensile Stress, in: R. Springenschmid (Ed.), Thermal Cracking in Concrete at Early Ages, RILEM Proceeding, E&FN Spon, London, 1995, pp. 111–118.
[8] M. Mangold, Methods for Experimental Determination of Thermal Stresses and Thermal Sensitivity in the Laboratory, in: R. Springenschmid (Ed.), Thermal Cracking in Concrete at Early Ages, RILEM Proceeding, E&FN Spon, London, 1995, pp. 26–39.
[9] H. Umehara, T. Uehara, Effect of Creep in Concrete at Early Ages on Thermal Stresses, Thermal Cracking in Concrete at Early Ages, in: R. Springenschmid (Ed.), Thermal Cracking in Concrete at Early Ages, RILEM Proceeding, E&FN Spon, London, 1995, pp. 79–86.
[10] G. Westman, Basic Creep and Relaxation of Young Concrete, in: R. Springenschmid (Ed.), Thermal Cracking in Concrete at Early Ages, RILEM Proceeding, E&FN Spon, London, 1995, pp. 87–94.
[11] Z.P. Bazant, Material Models for Structural Creep Analysis, in: Z.P. Bazant, J.F. Young (Eds.), RILEM Proc. Mathematical Modeling of Creep and Shrinkage of Concrete, John Wiley & Son, 1988.
[12] Z.P. Bazant, S.T. Wu, Dirichlet series creep function for aging concrete, ASCE J. Eng. Mech. (1973) 367–375.
[13] J.J. Brooks, A.M. Neville, A comparison of creep, elasticity, and strength of concrete in tension and in compression, Mag. Concr. Res. 29 (100) (1977) 131–141.
[14] J.M. Illston, The creep of concrete under uniaxial tension, Mag. Concr. Res. 17 (51) (1965) 77–84.
[15] A.A. Khan, W.D. Cook, D. Mitchell, Creep, shrinkage, and thermal strains in normal, medium, and high-strength concretes during hydration, ACI Mater. J. 94 (2) (1997) 156–166.
[16] L. Østergaard, D.A. Lange, S.A. Altoubat, H. Stang, Tensile basic creep of early-age concrete under constant load, Cem. Concr. Res. 31 (12) (2001) 1895–1899.
[17] E.A. Koenders, Simulation of volume changes in hardening cement-based materials, PhD Thesis, Delft Univ. Tech. (1997).
[18] S. Tangtermsirikul, Effect of chemical composition and particle size of fly ash on autogeneous shrinkage of paste, Proc. JCI Workshop Autog. Shrink. Conc. E \& FN Spon, Japan, 1999, pp. 175–182.
[19] Y.A. Abdel-Jawad, The relationships of cement hydration and concrete compressive strength to maturity, PhD Thesis, Univ. of Michigan (1988).
[20] Y. Peng, W. Hansen, C. Borgnakke, I. Pane, J.C. Romain, J. Biernacki, Thermo-kinetics of cement hydration – temperature effect and activation energy, in: Advances in concrete through science and engineering, Adv. Cement Based Mat. Int. Symposium.
[21] K.O. Kjellsen, R.J. Detwiler, Reaction kinetics of Portland cement mortar hydrated at different temperatures, Cem. Concr. Res. 22 (1) (1990) 112–120.
[22] K. Maekawa, R. Chaube, T. Kishi, Modeling of Concrete Performance: Hydration, Microstructure Formation, and Mass Transport, London, Routledge, 1999.
[23] N.J. Carino, The maturity method: theory and application, Cem. Conc. Agg. 6 (2) (1984) 61–73.
[24] N.J. Carino, H.S. Lew, C.K. Volz, Early age temperature effects on concrete strength prediction by maturity method, ACI J. 80 (3) (1983) 93–101.
[25] I. Pane, W. Hansen, Predictions and verifications of the early-age stress calculations in hydrating blended cement concrete, Cem. Concr. Res. 38 (11) (2008) 1315–1324.
[26] I. Pane, W. Hansen, Investigation of blended cement hydration by isothermal calorimetry and thermal analysis, Cem. Concr. Res. 35 (6) (2005) 1155–1164.
[27] S. Mindess, J.F. Young, Concrete, Prentice Hall, Englewood Cliffs, NJ, 1981.
[28] P.F. Hansen, E.J. Pedersen, Maleinstrument til kontrol of betons haerdning, Nordisk Betong 1 (1977) 21–29.
[29] I. Pane, W. Hansen, Concrete hydration and mechanical properties under nonisothermal conditions, ACI Mater. J. 99 (6) (2002) 534–542.
[30] A.M. Neville, W.H. Dilger, J.J. Brooks, Creep of Plain and Structural Concrete, Construction Press, New York, 1983.
[31] H. Morimoto, W. Koyanagi, Estimation of Stress Relaxation in Concrete at Early Ages, in: R. Springenschmid (Ed.), Thermal Cracking in Concrete at Early Ages, RILEM Proceeding, E&FN Spon, London, 1995, pp. 95–102.
[32] I. Carol, Z.P. Bazant, Viscoelasticity with aging caused by solidification of nonaging constituent, ASCE J. Eng. Mech. 119 (11) (1992) 2252–2269.
[33] Z.P. Bazant, Y. Xi, Continuous retardation spectrum for solidification theory of concrete creep, ASCE J. Eng. Mec. 121 (2) (1995) 281–288.
[34] N. Tschoegl, The Phenomenological Theory of Linear Viscoelastic Behavior: An Introduction, Springer-Verlag, 1989.
[35] J. Bensted, Special Cements, in: Peter C. Hewlett (Ed.), Lea's Chem, 4th ed., Cem. Conc., 1998.
[36] D. Lawrence, The Constitution and Specification of Portland Cements, in: Peter C. Hewlett (Ed.), Lea's Chem, 4th ed., Cem. Conc., 1998.
[37] O. Bjontegaard, Thermal dilation and autogeneous deformation as driving forces to self-induced stresses in high performance concrete, Doctoral Thesis, Norwegian Univ. Sci. Tec. Trondheim (1999).
[38] H. Hedlund, Stresses in high performance concrete due to temperature and moisture variations at early ages, Licentiate Thesis, Lulea University of technology, Sweden, 1996.